Prediction of Redox Potentials for the Late Actinides Cm to Lr Using Electronic Structure Methods

Felipe R. Dutra and David A. Dixon*

Cite This: *J. Phys. Chem. A* 2025, 129, 10717−10729

ABSTRACT: Our previously developed computational method for calculating the aqueous redox potentials of the early actinides has been extended to the later elements in the actinide series: Cm, Bk, Cf, Es, Fm, Md, No, and Lr in multiple oxidation states. These calculations were performed using density functional theory with small-core pseudopotentials and their associated basis sets. Solvation effects were considered via a supermoleculecontinuum approach, with 30 water molecules representing two solvation shells. Both the COSMO and SMD implicit solvation models were utilized. The structural parameters and hydration numbers for Cm(III), Bk(III), Bk(IV), and Cf(III) are in reasonable agreement with the available experimental data. For redox processes involving atomic cations in solution, the B3LYP/COSMO approach predicted redox potentials to within ±0.2 V of the experimental values for most redox couples, consistent with our prior work. Inclusion of spin−orbit corrections in specific redox pairs, especially those with the later actinides in high oxidation states, yields improved results relative to calculations including only scalar-relativistic corrections. The An^{+m}/An(0) redox potentials were calculated using a Born−Haber cycle incorporating sublimation, ionization, and hydration energies. Due to a lack of experimental data, three sets of ionization energies were used for the Born−Haber cycle. The calculated An(III/0) potentials showed better agreement with experimental data when using the COSMO solvation model and the test set comprising the NIST recommended ionization energies. The Md(II/0) potential was better described with the SMD model, whereas No(II/0) was not well described by all methods. The computational approach was able to predict redox potentials that for most cases agreed with the current available experimental or estimated data.

INTRODUCTION

The actinide series represents an important class of elements, characterized by compounds that display a remarkably diverse array of physical properties. Starting at americium (Am), the remaining actinides are purely synthetic elements. Cm, Bk, Cf, Es, Fm, Md, No, and Lr exhibit behavior similar to that of the lanthanides and do not exhibit as many oxidation states as the earlier actinides.[1] Understanding the accessible oxidation states of actinides is essential for gaining deeper insights into their chemical behavior and reactivity.[2] The complex electronic configurations of actinides allow for a variety of unusual oxidation states in the series, including the divalent state observed for Md(II) and No(II).[3] For the later actinides, the highest oxidation state experimentally confirmed in aqueous solution is +IV, via pulse radiolysis experiments.[4] Cf(IV) has been proposed based on a series of oxidation experiments in phosphotungstate solutions;[5] however, other experimental studies have failed to confirm the existence of such species, leaving their stability in solution uncertain.[6] The +V state for such elements could be accessed only in the gas phase as the $Cm(V)O_2^{+1}$ and $Bk(V)O_2^{+1}$ actinyl cations, and also as anionic nitrate complexes, $An(V)O_2(NO_3)^{2-}$.[7] Spitsyn and Ionova[8] proposed the possibility of Cm(V) and Cm(VI) in solution, but there have been no successful attempts in preparing such species due to the instability of Cm(V) in solution. The Cm(VI) state was claimed to be synthesized in carbonate solution as the ion CmO_2^{+2}, by β decay of Am-242. Domanov and Lobanov[9] synthesized Cm(VI) as volatile $Cm(VI)O_3$, by thermal oxidation of trace amounts of Cm hydrides. Later, Domanov[10] indicated the possibility of existing $Cm(VIII)O_4$ in the gas phase. Starting at Fm, even fewer states are claimed to be accessible only up to the +III state. The +II state becomes more important near the end of the actinide series, and is the most stable oxidation state for No. The Md(I) cation has been claimed to be obtained in some studies,[11] although its existence was questioned by others.[12,13] The final element of the actinide series, Lr, was only reported in aqueous solution as a Lr(III) cation.[14]

Since many oxidation states of these actinides are highly unstable in aqueous solutions, direct measurements are not feasible, and experimental redox data are available for only a limited number of redox couples. The significant instability of these states, combined with the presence of only trace amounts of such elements, makes obtaining their redox behavior particularly challenging. Many semiempirical approaches have been developed, enabling estimates for different redox

couples.[15–18]

Computational chemistry serves as a valuable tool for predicting the chemical characteristics of these elements, thereby aiding scientists in understanding their behavior in aqueous solutions. In previous studies, we successfully predicted standard reduction potentials for actinides, ranging from Ac to Am, across multiple oxidation states in acidic[19,20] and alkaline media.[21] Our approach uses thermodynamic cycles incorporating solvated ions within an extended solvation shell, together with an implicit self-consistent reaction field (SCRF) solvation model. Use of scalar-relativistic DFT with the B3LYP exchange-correlation functional in combination with a SCRF for solvation gave satisfactory predictions, differing from experiment by no more than ±0.2 V. In the current work, we have used this approach to predict standard reduction potentials in acidic aqueous environments for the later actinide elements Cm, Bk, Cf, Es, Fm, Md, No, and Lr for various oxidation states. We utilize density functional theory with explicit/implicit solvation models, employing the COSMO[22,2 1] and SMD[24] SCRF approaches.[25]

COMPUTATIONAL METHODS

Following our previous work,[19,20] the standard half-cell reduction potentials for the couples An(IV/III), An(III/II), and An(II/I) can be calculated using the standard thermodynamic cycle shown in Figure 1. We assume that the species in

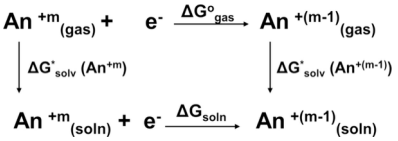

Figure 1. Thermodynamic cycles used for the predictions of An(IV/III), An(III/II), and An(II/I) reduction potentials.

[1] .[42,43] The Gibbs free energy of reduction can then be predicted by employing eq 4:

G_{soln} = $_{subl}$ G_{hyd}(An+m) (4) where ΔG_{subl} is the sublimation energy, I.E. is the ionization energy, and $\Delta G_{hyd}(An^{+m})$ is the hydration energy. The Gibbs free energies of sublimation were calculated using thermodynamic data, including the enthalpy of formation and absolute entropies in both gas and solid phases. The uncertainty in the enthalpy of sublimation values is higher for the later actinides, and the entropy values are based on estimates.[44] This approach yields ΔG_{subl} values of 82.7 (Cm), 65.4 (Bk), 38.3 (Cf), 23.1 (Es), 26 (Fm), 26 (Md), 25.6 (No), and 72.3 (Lr) kcal/mol. A

the gas phase and solution phase are at a state of 1 atm and 1 mol/L, respectively, and use the ion convention. The Gibbs free energy of this reduction reaction in solution is given by eq 1:

$$\Delta G_{soln} = \Delta G_{gaso} + \Delta G_{solv}^{*}(An^{-n}) - \Delta G_{solv}^{*}(An) \quad (1)$$

The full cell potential related to the standard hydrogen electrode can be calculated using eq 2:

$$E^{o}_{SHE} = -\frac{\Delta_{soln} G^{o}}{zF} \quad (2)$$

where z is the number of electrons transferred in the reaction, F is the Faraday constant, and E^{o}_{SHE} is the cell potential for the standard hydrogen electrode (SHE). The absolute value of the SHE adopted in this study is −4.28 V.[26] No thermodynamic correction for the electron is considered.

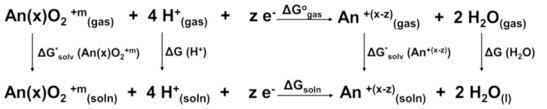

Figure 2. Thermodynamic cycle utilized for predicting the reduction potentials of actinyls reducing to atomic cations.

The redox processes involving the actinyls converting to solvated atomic cations is shown in Figure 2. For this case, the energy in solution is calculated using eq 3.

$$\Delta G_{soln} = \Delta G_{gaso} + \Delta G_{solv}^{*}(An) + 2\,\Delta G(H_2O) - \Delta G_{solv}^{*}(An) - 4\,\Delta G(H^{+}) \quad (3)$$

$\Delta G = -\Delta G - I.E. - \Delta G$ The value adopted for $\Delta G(H_2O)$ is −2.05 kcal/mol. The value of −262.4 kcal/mol for

number of ionization energies for the cations have not been determined experimentally, and the remaining energies have been estimated by extrapolation of known experimental data or obtained from electronic structure calculations. In this work, different sets of ionization energies were utilized: (i) combining the experimentally known and estimated ionization energies recommended by the NIST database; (ii) relying on experimentally known and the computed data from Feng and Peterson;[45] and (iii) a combination of experimental data and energies calculated by Pantazis and Neese.[46] No entropic corrections were applied to this energy, as other studies

1. Gas Phase Enthalpies and Gibbs Free Energies in the Gas Aqueous Phases Calculated at the B3LYP/ECP(60)/ TZVP Level for the Prediction of the Number of H_2O Molecules in the 1st Coordination Shell in kcal/mol

Species	Spin	Shell transfer	ΔH_{gas}	ΔG_{gas}	ΔG_{soln} COSMO	ΔG_{soln} SMD
Cm(I)	8	8/22 → 7/23	−1.16	−2.25	−5.67	−10.00
Cm(II)	7	8/22 → 7/23	−0.65	0.09	−1.06	−4.65
Cm(III)	8	9/21 → 8/22	−0.24	9.17	0.16	−2.94
Cm(IV)	7	9/21 → 8/22	−3.91	−4.20	−5.14	−3.46
$Cm(V)O_2^{+1}$	6	5/25 → 4/26	5.84	2.51	−2.95	−9.17
$Cm(VI)O_2^{+2}$	5	5/25 → 4/26	7.03	3.50	1.82	−6.96
Bk(I)	7	8/22 → 7/23	−7.40	−6.00	−1.83	−6.54
Bk(II)	6	8/22 → 7/23	15.54	13.34	1.00	−4.68
Bk(III)	7	9/21 → 8/22	3.80	9.88	1.61	−2.70
Bk(IV)	8	9/21 → 8/22	0.49	4.17	−8.75	−12.47
$Bk(V)O_2^{+1}$	7	5/25 → 4/26	7.63	3.60	−2.48	−10.01
Cf(I)	6	8/22 → 7/23	−0.28	−0.36	−5.38	−8.70
Cf(II)	5	8/22 → 7/23	−0.50	1.07	−0.86	−7.69
Cf(III)	6	9/21 → 8/22	−9.63	−1.41	−7.29	−8.40
Cf(IV)	7	9/21 → 8/22	4.74	7.92	−7.51	−10.63
$Cf(V)O_2^{+1}$	8	5/25 → 4/26	12.40	8.58	1.80	−7.23
Es(I)	5	8/22 → 7/23	−0.01	−0.21	−2.60	−9.17
Es(II)	4	8/22 → 7/23	−3.96	−2.41	0.80	−3.42
Es(III)	5	9/21 → 8/22	−10.86	−2.44	−5.67	−6.81
Es(IV)	6	8/22[a]				
Fm(I)	4	8/22 → 7/23	−3.00	−2.80	−3.17	−7.88
Fm(II)	3	8/22 → 7/23	14.73	12.88	0.14	−3.30
Fm(III)	4	9/21 → 8/22	−10.51	−2.54	−4.84	−5.02
Md(I)	3	8/22 → 7/23	−5.30	−5.07	−5.35	−10.07
Md(II)	2	8/22 → 7/23	3.44	3.45	−3.29	−4.54
Md(III)	3	9/21 → 8/22	−12.36	−4.21	−9.77	−11.40
No(I)	2	8/22 → 7/23	1.69	0.33	−2.52	−5.45
No(II)	1	8/22 → 7/23	−1.87	−4.25	−1.78	−4.40
No(III)	2	9/21 → 8/22	−13.74	−5.35	−11.25	−10.69
Lr(II)	2	8/22 → 7/23	−2.97	−3.67	−5.68	−15.94
Lr(III)	1	9/21 → 8/22	−12.83	−5.51	−9.68	−11.42

[a] 9/21 structures optimized to 8/22 structures.

the proton, which considers the change of 1 atm to 1 mol/L, is used in this work although a value of −264.3 kcal/mol has also provided good results for a variety of pK_a predictions.[27−30]

The cluster geometries in this study were optimized using density functional theory (DFT)[31] level with the B3LYP exchange-correlation functional[32,33] as implemented in the Gaussian16 software.[34] All calculations employed the quadratically convergent (XQC) algorithm. The DFT optimized TZVP basis set was used for the oxygen and hydrogen atoms,[35] and the Stuttgart small-core relativistic effective core potentials (60ECP) together with the associated segmented basis sets were used for the actinides.[36−39] The frequencies were adjusted using the Goodvibes program,[40] which applies a scaling factor to account for anharmonicity, depending on the level of theory/basis set used, and adjusts vibrational modes lower than 100 cm^{-1} to 100 cm^{-1} following Truhlar and co-workers.[41]

As described previously,[19−21] the An^{+m}/An(0) potentials can be predicted utilizing a Born−Haber cycle depicted in Figure

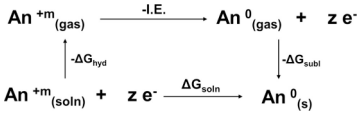

Figure 3. Born−Haber cycle used for the predictions of An(IV/0), An(III/0), An(II/0), and An(I/0) reduction potentials.

demonstrate that their impact is minimal.[43] The energies used for each set are described in the Supporting Information (SI). The hydration free energy, $\Delta G_{hyd}(An^{+m})$, can be determined using reaction 5.

$$An^{+m}(gas) + (H_2O)_n(aq) \rightarrow An^{+m}(H_2O)_n(aq) \quad (5)$$

The hydration free energies can be calculated by combining the gas phase free energy of the reaction and the bulk solvent shift, using eq 6. The gas phase free energies for the hydration reaction are calculated using eq 7.

$$\Delta G_{hyd}(An_{+m}) = \Delta G_{gas}(An_{+m}(H_2O)_n) + \Delta\Delta G_{solv}(An_{+m}(H_2O)_n) \quad (6)$$

$$\Delta G_{gas}(An_{+m}(H_2O)_n) = G_{gas}(An_{+m}(H_2O)_n) - G_{gas}(An_{+m}) - G_{gas}((H_2O)_n) \quad (7)$$

The bulk solvent shift $\Delta\Delta G_{solv}$ can be calculated using eq 8.

$$\Delta\Delta G_{solv}(An_{+m}(H_2O)_n) = \Delta G_{solv}(An_{+m}(H_2O)_n) - \Delta G_{solv}((H_2O)_n) \quad (8)$$

In this case, the standard state correction of −4.27/n kcal/mol for each water $(H_2O)_n$ cluster was not included, due to the small impact on the energetics when clusters of this size are used. The potentials for An(IV/0), An(III/0), An(II/0), and An(I/0) can be calculated in a similar manner (Figure 3) and using eq 2, considering the number of electrons transferred.

The solvation energies were calculated using two implicit

Table 2. Comparison between Averaged Experimental and Calculated Bond Lengths R(An−OH_2) for the Solvated Actinide Ions Calculated at the B3LYP/ECP(60)/TZVP Level (CNs Are in Parentheses; All Values Are in Å)

Species	Spin	Calc. current	Other Calc. DFT	Other Calc. MD/MC	Expt. 1 M [H^+]
Cm(III)	8	2.49(8), 2.54(9)	2.445(8),[73] 2.473(9),[73] 2.526(8),[67] 2.566(9)[67]	2.46(9.0),[65,66] 2.55(8.9),[74] 2.48(9.0)[75]	2.45(10.2),[70] 2.48(8.5),[76] 2.47(9.0)[77]
Cm(IV)	7	2.50(8)	2.34(8)[82]	2.32(8.9),[81] 2.34(8.9)[81]	
Bk(III)	7	2.47(8), 2.52(9)	2.511(8),[67] 2.551(9)[67]	2.44(9.0),[65] 2.43(9.0)[66]	2.43(9.0)[78]
Bk(IV)	8	2.35(8)	2.33(8)[82]	2.34(9.5),[81] 2.34(8.9)[81]	2.32(7.9)[78]
Cf(III)	6	2.45(8), 2.50(9)	2.495(8),[67] 2.537(9)[67]	2.42(9.0)[65]	2.42(8.5)[79,80]
Es(III)	5	2.44(8), 2.49(9)	2.482(8),[67] 2.524(9)[67]	2.37(8.5)[66]	
Fm(III)	4	2.43(8), 2.49(9)	2.469(8),[67] 2.513(9)[67]	2.35(8.3)[66]	
Md(III)	3	2.42(8), 2.48(9)	2.455(8),[67] 2.502(9)[67]	2.34(8.1)[66]	
No(II)	1	2.57(7), 2.62(8)	2.59(8)[64]	2.55(7.46)[64]	
No(III)	2	2.41(8), 2.48(9)	2.443(8),[67] 2.490(9)[67]	2.32(8.0)[66]	
Lr(III)	1	2.40(8), 2.47(9)	2.431(8),[67] 2.479(9)[67]	2.31(8.0)[66]	

solvent models, COSMO[22,23] and SMD.[24] The explicit/ implicit solvation model used in the current study follows the same approach as in our previous work,[19−21] where actinides were embedded in clusters containing 30 water molecules distributed across two solvation layers. In the $An^{n+}(H_2O)_x(H_2O)_y$ clusters, the distinct H_2O in parentheses define the number of explicit waters in each solvation shell. For the tetravalent and trivalent oxidation states, values of x = 8 or 9 were used for the first solvation shell, and corresponding values of y = 22 or 21, respectively, were used for the second solvation shell for a total of 30 H_2O. For the divalent and monovalent states, values of x = 7 or 8, and associated values of y = 23 or 22, respectively, were used. For the actinyls $AnO_2^{n+}(H_2O)_x(H_2O)_y$ clusters, values of x = 4 or 5, and corresponding values of y = 26 or 25, respectively, were used. Spin−orbit calculations were performed for both the bare and solvated systems using the ADF code,[47,48] employing the ZORA spin−orbit formalism[49−53] at the BLYP/TZ2P level.[54,55] The spin−orbit correction was determined as the energy difference between the ZORA and ZORA+SO results. In the current work, the clusters were optimized without imposing any symmetry constraints to find the lowest energy geometry. Configurational sampling across the entire accessible space[56,57] is too computationally demanding because of the numerous degrees of freedom associated with the loosely bound water molecules. Our group has employed a supermolecule-continuum method with varying numbers of explicit solvent molecules selected according to the specific system studied. This approach has been successfully applied to a wide range of redox potentials for both cations and anions, yielding excellent agreement with experimental values, typically within 0.2 V, and often significantly better.[19−21,58−61] This computational approach is appropriate for systems at infinite dilution (ionic strength = 0), as no counterions are included in our simulations. Overall, the results obtained using our approach differ from experiment by a magnitude comparable to that of much more computationally intensive techniques, such as ab initio molecular dynamics (AIMD) based on density functional theory combined with free energy perturbation or thermodynamic integration methods to evaluate the free energy of electron insertion (i.e., the work function).[56,57] It is also worth noting that the DFT/thermodynamic integration approach[56] has been reported to encounter difficulties when the excited states of the solute approach the edges of the water band gap, a limitation that is not present in our method.

RESULTS AND DISCUSSION

First Shell Coordination Number. Table 1 provides the energies associated with changes in the coordination number (CN) within the primary solvation shell. The small energetic differences in these solvent shift reactions suggest that numerous coordination possibilities can coexist. Very little, if any, experimental information about hydration shell sizes is available for the later elements of the actinide series, mostly due to their instability and short half-lives, with reliable data only available up to Cf. Our optimized structures for the monovalent oxidation states have CN = 7 for all actinides. Through comparison of the available cationic radii, David et al.[62] observed that divalent plutonium and transplutonium elements have ionic radii comparable to those of alkaline earth dications. Given the CN of 6 for the earlier Group 2 dications, they speculated that An(II) cations might also adopt the same CN. Applying the same methodology, they estimated that monovalent actinide species would likely exhibit a CN of 4, trivalent species a CN of 8, and tetravalent species a CN of 8 or 9. Subsequently, David[63] estimated that the hydration number decreases proportionally with the ionic charge and along the actinide series. In a recent study, Watanabe et al.[64] performed DFT and DFT-MD simulations to investigate the hydration structure of No(II) in aqueous solution. Their results suggested smaller hydration numbers, with CN of 7 or 8 coexisting for this cation. Our calculations predict that No(II) and some of the divalent actinides prefer CN = 7 when using the COSMO solvation model, whereas the SMD model consistently favors CN = 8 for all actinides. However, the energy differences between these configurations are small, suggesting that both structures may coexist in solution. As in our previous work,[19−21] we chose the geometries predicted by the COSMO model.

D'Angelo et al.[65] studied the hydration numbers and ionic radii of trivalent actinides using a combination of EXAFS and molecular dynamics, extending their analysis up to Cf. They observed a gradual decrease in An−OH_2 bond length across the series, with the coordination number remaining largely unchanged at 9. Duvail et al.[66] performed molecular dynamics simulations for all trivalent actinide cations and reported

3. Cm, Bk, Cf, Es, Fm, Md, No, Lr in Different Oxidation States in Aqueous Solution Calculated at the B3LYP/ECP(60)/TZVP Level (Potentials in Volts Relative to SHE)

An(ox)	Spin	An(red)	Spin	E° COSMO	E° SMD	E° expt	E° est
$Cm(H_2O)_7(H_2O)_{23+2\sigma}$	7	$Cm(H_2O)_7(H_2O)_{23+1\sigma}$	8	−2.25	−2.56		
$Cm(H_2O)_9(H_2O)_{21+3}$	8	$Cm(H_2O)_7(H_2O)_{23+2\sigma}$	7	−2.86	−2.44	−2.78[83]	−3.50,[2] −4.4,[16] −3.3[17]
$Cm(H_2O)_8(H_2O)_{22+4}$	7	$Cm(H_2O)_9(H_2O)_{21+3}$	8	3.13	2.64		3.5,[16] 3.0[17]
$Cm(V)O_2(H_2O)_4(H_2O)_{26+1\sigma}$	6	$Cm(H_2O)_9(H_2O)_{21+3}$	8	2.84	2.93		
$Cm(V)O_2(H_2O)_4(H_2O)_{26+1\sigma}$	6	$Cm(H_2O)_8(H_2O)_{22+4}$	7	2.55	3.22		1.70,[8] 1.60[92]
$Cm(VI)O_2(H_2O)_5(H_2O)_{25+2\sigma}$	5	$Cm(H_2O)_9(H_2O)_{21+3}$	8	2.68	2.82		
$Cm(VI)O_2(H_2O)_5(H_2O)_{25+2\sigma}$	5	$Cm(H_2O)_8(H_2O)_{22+4}$	7	2.46	2.91		
$Cm(VI)O_2(H_2O)_5(H_2O)_{25+2\sigma}$	5	$Cm(V)O_2(H_2O)_4(H_2O)_{26+1\sigma}$	6	2.20	2.44		1.50,[8] 1.60[92]
$Bk(H_2O)_8(H_2O)_{22+2\sigma}$	6	$Bk(H_2O)_7(H_2O)_{23+1\sigma}$	7	−3.14	−2.99		
$Bk(H_2O)_9(H_2O)_{21+3}$	7	$Bk(H_2O)_8(H_2O)_{22+2\sigma}$	6	−2.02	−2.32	−2.52[83]	−2.80[16,17]
$Bk(H_2O)_8(H_2O)_{22+4}$	8	$Bk(H_2O)_9(H_2O)_{21+3}$	7	1.97	1.68	1.67[2]	1.60[16,17]
$Bk(V)O_2(H_2O)_4(H_2O)_{26+1\sigma}$	7	$Bk(H_2O)_8(H_2O)_{22+3}$	7	2.13	2.13		
$Bk(V)O_2(H_2O)_4(H_2O)_{26+1\sigma}$	7	$Bk(H_2O)_8(H_2O)_{22+4}$	8	2.30	2.58		3.30,[92] 3.5[18]
$Cf(H_2O)_7(H_2O)_{23+2\sigma}$	5	$Cf(H_2O)_7(H_2O)_{23+1\sigma}$	6	−3.10	−3.32		
$Cf(H_2O)_8(H_2O)_{22+3}$	6	$Cf(H_2O)_7(H_2O)_{23+2\sigma}$	5	−1.56	−1.67	−1.63[83]	−1.60[16,17]
$Cf(H_2O)_8(H_2O)_{22+4\sigma}$	7	$Cf(H_2O)_8(H_2O)_{22+3}$	6	2.89	2.67		3.20[16,17]
$Cf(V)O_2(H_2O)_5(H_2O)_{25+1\sigma}$	8	$Cf(H_2O)_8(H_2O)_{22+3}$	6	3.05	3.21		
$Cf(V)O_2(H_2O)_5(H_2O)_{25+1\sigma}$	8	$Cf(H_2O)_8(H_2O)_{22+4\sigma}$	7	3.76	3.22		1.00[92]
$Es(H_2O)_8(H_2O)_{22+2\sigma}$	4	$Es(H_2O)_7(H_2O)_{23+1\sigma}$	5	−3.22	−3.07		
$Es(H_2O)_8(H_2O)_{22+3}$	5	$Es(H_2O)_8(H_2O)_{22+2\sigma}$	4	−1.23	−1.47	−1.45[83]	−1.30[16,17]
$Es(H_2O)_8(H_2O)_{22+4\sigma}$	6	$Es(H_2O)_8(H_2O)_{22+3}$	5	3.72	3.48		4.50[16,17]
$Fm(H_2O)_8(H_2O)_{22+2\sigma}$	3	$Fm(H_2O)_7(H_2O)_{23+1\sigma}$	4	−3.19	−3.13		
$Fm(H_2O)_8(H_2O)_{22+3}$	4	$Fm(H_2O)_8(H_2O)_{22+2\sigma}$	3	−0.67	−0.96	−1.18[83]	−1.20,[2] −1.10[16,17]
$Md(H_2O)_7(H_2O)_{23+2}$	2	$Md(H_2O)_7(H_2O)_{23+1\sigma}$	3	−3.29	−3.28		
$Md(H_2O)_8(H_2O)_{22+3}$	3	$Md(H_2O)_7(H_2O)_{23+2}$	2	0.29	0.09	−0.15,[83] −0.16[84]	0.0,[16] −0.20[17]
$No(H_2O)_7(H_2O)_{23+2}$	1	$No(H_2O)_7(H_2O)_{23+1\sigma}$	2	−3.35	−3.44		
$No(H_2O)_8(H_2O)_{22+3}$	2	$No(H_2O)_7(H_2O)_{23+2}$	1	1.56	1.42	1.45[83]	1.30[16,17]
$Lr(H_2O)_8(H_2O)_{22+3}$	1	$Lr(H_2O)_7(H_2O)_{23+2\sigma}$	2	−2.93	−2.65	<−0.44[14]	−2.60[17]

σ Species not reported experimentally.

average CN between 8 and 9, depending on the element. In a previous computational study by Wiebke et al.[67] at the DFT level, all An(III) ions favor CN = 8, whereas at the MP2 level, CN = 9 for all actinides, except No(III) and Lr(III). The Cm(III) ion has been extensively explored, and several studies reported CN from 8 to 10 waters,[68−76] whereas the most recent EXAFS analysis suggests a preference for CN = 9.[77] Our calculations indicate a small preference for the CN = 9 structure for Cm(III) when using the COSMO solvation model, whereas SMD favored CN = 8. Antonio et al.[78] performed an XAS analysis of Bk ions in solution, and indicated that Bk(III) prefers CN = 9, whereas Bk(IV) favors CN = 8. Our calculations favor these specific CN as well when using the COSMO solvation model. For Cf(III), Revel et al.[79] performed EXAFS experiments, and Galbis et al.[80] combined Monte Carlo simulations with EXAFS analysis; both found that Cf(III) manifests as two structures, with CN = 8 and 9, pointing out a slight preference for the former. Our calculations indicate that CN = 8 is favorable for Cf(III), using both solvation models.

Acher et al.[81] conducted molecular dynamics studies on multiple tetravalent actinides using two different force fields and obtained varying results. For Cm(IV), the average CN ranged from 8.3 to 8.9, whereas for Bk(IV), the average CN ranged from 8.9 to 9.5. Banik et al.[82] used computational methods to suggest a preference of CN = 8 for Cm(IV) and Bk(IV). Our calculations indicate that not only these cations, but all the heavier tetravalent actinides favor CN = 8.

There are no experimental or computational studies for actinyls of the later actinides. Our calculations demonstrate that the pentavalent actinides favor CN = 4, except for $Cf(V)O_2^{+1}$, which favors CN = 5, and the hexavalent $Cm(VI)O_2^{+2}$ favor CN = 5.

Structural Parameters. Table 2 presents the average bond distances between the actinides and water molecules. Most of the available data is for trivalent and tetravalent in aqueous solution, except for No(II). For Cm(III), the calculated distances for CN = 8 are in better agreement with the experimental data, even though the CNs are not in agreement. With CN = 9, our values for Cm(III) are 0.07 Å longer than the experimental data from Skanthakumar et al.[77] and relatively close to the values provided in computational studies by Wiebke et al.[67] and Hagberg et al.[74] For the Cm(IV) ion, our calculated values differ significantly (0.16 Å longer) from the values calculated by Banik et al.[82]

For Bk(III) and Bk(IV), our calculations predicted longer bonds than found experimentally. For Bk(III) (CN = 9), the bonds are 0.09 Å longer and for Bk(IV) (CN = 8) 0.03 Å longer than the values obtained by Antonio et al.[78] For Cf(III), our calculations with CN = 8 are in agreement with the experimental values,[79,80] differing by only 0.03 Å. The bond distances calculated for the remaining An(III) cations are generally longer than the simulations performed by Duvail et al.,[66] with CN = 8 usually differing by more than 0.05 Å; our values are closer to the DFT results obtained by Wiebke et al.[67] For No(II) (CN = 7), our bond distances are similar to the results obtained by Watanabe et al.,[64] differing by 0.02 Å from

https://doi.org/10.1021/acs.jpca.5c06523
J. Phys. Chem. A 2025, 129, 10717−10729

$Cm(H_2O)_7(H_2O)_{23+1}$[a]	8	Cm	0.51	0.51	0.51	−1.02	−1.02	−1.02		
$Cm(H_2O)_7(H_2O)_{23+2}$[a]	7	Cm	−0.79	−0.82	−0.74	−1.72	−1.74	−1.67		−1.38[17]
$Cm(H_2O)_9(H_2O)_{21+3}$	8	Cm	−1.87	−1.83	−1.64	−2.34	−2.31	−2.12	−2.06[85]	−2.02[17]
$Cm(H_2O)_8(H_2O)_{22+4}$	7	Cm	−1.23	−1.20	−0.68	−1.72	−1.70	−1.17		−0.77[17]
$Bk(H_2O)_7(H_2O)_{23+1}$[a]	7	Bk	1.20	1.20	1.20	0.11	0.11	0.11		
$Bk(H_2O)_8(H_2O)_{22+2}$[a]	6	Bk	−1.23	−1.22	−1.03	−1.70	−1.68	−1.49		−1.56[17]
$Bk(H_2O)_9(H_2O)_{21+3}$	7	Bk	−1.85	−1.77	−1.47	−2.26	−2.18	−1.88	−2.00[86]	−1.98[17]
$Bk(H_2O)_8(H_2O)_{22+4}$	8	Bk	−1.23	−1.16	−0.82	−1.61	−1.54	−1.20		−1.08[17]
$Cf(H_2O)_7(H_2O)_{23+1}$[a]	6	Cf	3.81	3.84	4.04	3.34	3.37	3.57		
$Cf(H_2O)_7(H_2O)_{23+2}$[a]	5	Cf	−1.83	−1.80	−1.60	−2.41	−2.38	−2.18		−2.10[17]
$Cf(H_2O)_8(H_2O)_{22+3}$	6	Cf	−2.10	−1.88	−1.55	−2.52	−2.30	−1.97	−1.92[87]	−1.95[17]
$Cf(H_2O)_8(H_2O)_{22+4}$[a]	7	Cf	−1.03	−0.86	−0.42	−1.40	−1.24	−0.79		−0.65[17]
$Es(H_2O)_7(H_2O)_{23+1}$[a]	5	Es	−1.27	−1.27	−1.27	−2.34	−2.34	−2.34		
$Es(H_2O)_8(H_2O)_{22+2}$[a]	4	Es	−2.44	−2.45	−2.25	−2.90	−2.90	−2.71		−2.24[17]
$Es(H_2O)_8(H_2O)_{22+3}$	5	Es	−2.23	−2.04	−1.55	−2.62	−2.42	−1.93	−1.98[88]	−1.91[17]
$Fm(H_2O)_7(H_2O)_{23+1}$[a]	4	Fm	−0.18	−0.53	−0.23	−1.07	−1.42	−1.12		
$Fm(H_2O)_8(H_2O)_{22+2}$[a]	3	Fm	−1.84	−2.06	−1.71	−2.27	−2.48	−2.13		−2.31[17]
$Fm(H_2O)_8(H_2O)_{22+3}$	4	Fm	−2.27	−2.21	−1.57	−2.64	−2.58	−1.95	−2.07[89]	−1.89[17]
$Md(H_2O)_7(H_2O)_{23+1}$[a]	3	Md	−0.06	−0.41	−0.10	−1.02	−1.37	−1.06		
$Md(H_2O)_7(H_2O)_{23+2}$	2	Md	−1.91	−2.06	−1.70	−2.38	−2.53	−2.17	−2.50[2]	−2.37[17]
$Md(H_2O)_8(H_2O)_{22+3}$	3	Md	−1.70	−1.55	−0.86	−2.08	−1.93	−1.25	−1.74[90]	−1.64[17]
$No(H_2O)_7(H_2O)_{23+1}$[a]	2	No	0.07	0.07	0.08	−0.87	−0.87	−0.86		
$No(H_2O)_7(H_2O)_{23+2}$	1	No	−1.68	−1.85	−1.64	−2.19	−2.37	−2.16	−2.61[91]	−2.47[17]
$No(H_2O)_8(H_2O)_{22+3}$	2	No	−1.09	−0.96	−0.43	−1.48	−1.35	−0.82	−1.26[90]	−1.21[17]
$Lr(H_2O)_7(H_2O)_{23+2}$[a]	2	Lr	−1.01	−1.02	−1.01	−1.74	−1.76	−1.75		−1.51[17]
$Lr(H_2O)_8(H_2O)_{22+3}$	1	Lr	−1.74	−1.78	−1.69	−2.14	−2.18	−2.09	−2.06[92]	−1.89[17]

[a] Species not reported experimentally. [b] I.E. values extracted from the NIST database. [c] I.E. values extracted from experimentally known and the

4. Cm, Bk, Cf, Es, Fm, Md, No, and Lr in Different Oxidation States Reducing to the Metal Calculated at the B3LYP/ECP(60)/TZVP Level Using Different Sets for Ionization Energies (Potentials in Volts Relative to SHE)

An(ox)	Spin	E° COSMO				E° SMD				E° est
		An[0]	I[b]	II[c]	III[d]	I[b]	II[c]	III[d]	E° expt	

computed data from Feng and Peterson.[45] [d] I.E. values extracted from experimentally known and the computed data from Pantazis and Neese.[46]

Table 5. Calculated Spin−Orbit Effects on the Ionization Energies for Solvated and Bare Species Calculated in ZORA-BLYP/ TZ2P in kcal/mol

Solvated Ions					Bare Ions				
An	Spin	An^+	Spin	ΔSO	An	Spin	An^+	Spin	ΔSO
$Cm(H_2O)_7(H_2O)_{23+2}$	7	$Cm(H_2O)_7(H_2O)_{23+1}$	8	0.0	Cm_{2+}	7	Cm_{1+}	8	−4.7
$Cm(H_2O)_9(H_2O)_{21+3}$	8	$Cm(H_2O)_7(H_2O)_{23+2}$	7	0.8	Cm_{3+}	8	Cm_{2+}	7	6.0
$Cm(H_2O)_8(H_2O)_{22+4}$	7	$Cm(H_2O)_9(H_2O)_{21+3}$	8	0.3	Cm_{4+}	7	Cm_{3+}	8	−10.6
$Bk(H_2O)_8(H_2O)_{22+2}$	6	$Bk(H_2O)_7(H_2O)_{23+1}$	7	−0.6	Bk_{2+}	6	Bk_{1+}	7	−11.2
$Bk(H_2O)_9(H_2O)_{21+3}$	7	$Bk(H_2O)_8(H_2O)_{22+2}$	6	0.6	Bk_{3+}	7	Bk_{2+}	6	10.5
$Bk(H_2O)_8(H_2O)_{22+4}$	8	$Bk(H_2O)_9(H_2O)_{21+3}$	7	0.4	Bk_{4+}	8	Bk_{3+}	7	2.5
$Cf(H_2O)_7(H_2O)_{23+2}$	5	$Cf(H_2O)_7(H_2O)_{23+1}$	6	0.6	Cf_{2+}	5	Cf_{1+}	6	3.5

the DFT results and the molecular dynamics simulations. Overall, our results tend to predict slightly longer bond lengths
as compared to experimental data and molecular simulations, and are consistent with most DFT studies.

about the validity of this data. In addition, Nugent et al.[16] and Bratsch and Lagowski[17] reported potentials using empirical approaches. For the Cm(III/II) couple, both the COSMO and SMD results are consistent with the −2.78 V potential obtained by Mikheev et al.[83] For Bk(III/II), only the

6. Cm, Bk, Cf, Es, Fm, Md, No, Lr in Different Oxidation States in Aqueous Solution Calculated at the B3LYP/ECP(60)/TZVP Level and Incorporating **Δ**SO (Potentials in Volts Relative to SHE)

An(ox)	Spin	An(red)	Spin	E° COSMO	E° SMD	E° expt	E° est
$Cm(H_2O)_7(H_2O)_{23+2a}$	7	$Cm(H_2O)_7(H_2O)_{23+1a}$	8	−2.25	−2.56		
$Cm(H_2O)_9(H_2O)_{21+3}$	8	$Cm(H_2O)_7(H_2O)_{23+2a}$	7	−2.83	−2.41	−2.78[83]	−3.50,[2] −4.4,[16] −3.3[17]
$Cm(H_2O)_8(H_2O)_{22+4}$	7	$Cm(H_2O)_9(H_2O)_{21+3}$	8	3.14	2.65		3.5,[16] 3.0[17]
$Bk(H_2O)_8(H_2O)_{22+2a}$	6	$Bk(H_2O)_7(H_2O)_{23+1a}$	7	−3.17	−3.02		
$Bk(H_2O)_9(H_2O)_{21+3}$	7	$Bk(H_2O)_8(H_2O)_{22+2a}$	6	−1.99	−2.29	−2.52[83]	−2.80[16,17]
$Bk(H_2O)_8(H_2O)_{22+4}$	8	$Bk(H_2O)_9(H_2O)_{21+3}$	7	1.99	1.70	1.67[2]	1.60[16,17]
$Cf(H_2O)_7(H_2O)_{23+2a}$	5	$Cf(H_2O)_7(H_2O)_{23+1a}$	6	−3.07	−3.29		
$Cf(H_2O)_8(H_2O)_{22+3}$	6	$Cf(H_2O)_7(H_2O)_{23+2a}$	5	−1.66	−1.77	−1.63[83]	−1.60[16,17]
$Cf(H_2O)_8(H_2O)_{22+4a}$	7	$Cf(H_2O)_8(H_2O)_{22+3}$	6	2.92	2.70		3.20[16,17]
$Es(H_2O)_8(H_2O)_{22+2a}$	4	$Es(H_2O)_7(H_2O)_{23+1a}$	5	−3.22	−3.07		
$Es(H_2O)_8(H_2O)_{22+3}$	5	$Es(H_2O)_8(H_2O)_{22+2a}$	4	−1.44	−1.68	−1.45[83]	−1.30[16,17]
$Es(H_2O)_8(H_2O)_{22+4a}$	6	$Es(H_2O)_8(H_2O)_{22+3}$	5	3.69	3.45		4.50[16,17]
$Fm(H_2O)_8(H_2O)_{22+2a}$	3	$Fm(H_2O)_7(H_2O)_{23+1a}$	4	−3.10	−3.04		
$Fm(H_2O)_8(H_2O)_{22+3}$	4	$Fm(H_2O)_8(H_2O)_{22+2a}$	3	−0.85	−1.14	−1.18[83]	−1.20,[2] −1.10[16,17]
$Md(H_2O)_7(H_2O)_{23+2}$	2	$Md(H_2O)_7(H_2O)_{23+1a}$	3	−3.00	−2.99		
$Md(H_2O)_8(H_2O)_{22+3}$	3	$Md(H_2O)_7(H_2O)_{23+2}$	2	−0.08	−0.28	−0.15,[83] −0.16[84]	0.0,[16] −0.20[17]
$No(H_2O)_7(H_2O)_{23+2}$	1	$No(H_2O)_7(H_2O)_{23+1a}$	2	−3.35	−3.44		
$No(H_2O)_8(H_2O)_{22+3}$	2	$No(H_2O)_7(H_2O)_{23+2}$	1	1.15	1.01	1.45[83]	1.30[16,17]
$Lr(H_2O)_8(H_2O)_{22+3}$	1	$Lr(H_2O)_7(H_2O)_{23+2a}$ [a]	2	−3.11	−2.83	<−0.44[14]	−2.60[17]

[a] Species not reported experimentally.

Redox Potentials. Table 3 gives the redox potentials calculated in this work involving one electron processes for the cations in aqueous solution. Table 4 gives the redox potentials for the processes involving the reduction of cations to the metals. The redox potentials were compared to the experimental data[83−92] when available or to estimated values.[8,14,16,17]

For the An(II/I) redox potentials, our calculations indicate that these potentials are extremely negative for all actinides in the current study. Although no experimental data is available for comparison, the negative potentials indicate that the reduction process to the monovalent state is unfavorable, consistent with the well-known instability of this state for actinides.

In the case of An(III/II) potentials, Mikheev et al.[83] reported redox potentials obtained using a cocrystallization experimental technique, but David[63] has raised concerns

potentials calculated using the SMD model are consistent with experiment, differing by +0.20 V from the experimental value[83] of −2.52 V, whereas the COSMO value differs by 0.50 V from experiment. The predicted Cf(III/II) redox potentials agreed with the experimental data[83] and estimates of −1.60 V.[16,17] For Es(III/II), our calculations agree with the experimental data of Mikheev et al.[83] for both COSMO and SMD. In the case of Fm(III/II), only SMD yielded results within acceptable accuracy with experiment.[83] Similarly, for the Md(III/II) couple, the reduction potential calculated using SMD shows better agreement with the experimental value,[83,84] differing by +0.24 V, although it predicts a slightly positive potential. In contrast, the COSMO model yields a larger deviation of +0.44 V. The predictions for the No(III/II) redox couple provided satisfactory results with both solvation models, differing by +0.11 V with COSMO and −0.03 V with SMD. The calculated Lr(III/II) potential was substantially more negative than the reported upper limit,[14]

https://doi.org/10.1021/acs.jpca.5c06523
J. Phys. Chem. A 2025, 129, 10717−10729

and produced results in accordance with the estimated value.[17]

An experimental An(IV/III) potential is only available for Bk.[2] The predicted Cm(IV/III) redox couple agrees with the estimate[17] of +3.0 V, independent of the solvation model, with the COSMO result closer to this value. Our calculations for the Bk(IV/III) couple also predicted potentials in reasonable agreement with the literature,[2,16,17] with SMD in better agreement. For Cf and Es, our computational results differ from previously reported estimates,[16,17] yielding less positive reduction potentials. The calculated Cf(IV/III) reduction potential is approximately +2.8 V, and the Es(IV/III) potential is predicted to be in the range of +3.6 V.

Higher oxidation states than +IV have not been reported experimentally in solution for the later actinides. It is expected that the redox potentials would be extremely positive, reflecting the inherent instability of such oxidation states. Our calculations support this trend. The Cm(V/IV) potential was calculated to be 2.55 V using the COSMO solvation model and 3.22 V with the SMD model. Spitsyn and Ionova[8] developed a model by correlating the energies of electronic transitions involving the 5f electrons of Cm and estimated a potential of 1.7 V for Cm(V/IV). Our calculated values differ significantly from this estimate and are more positive. Similarly, Cm(VI/V) was predicted to be ∼2.5 V, in contrast to the estimated value of 1.5 V from Spitsyn and Ionova.[8] In contrast to their conclusions, our results indicate that it is very unlikely that such cations can form in noncomplexing aqueous media. The Bk(V/IV) calculated potential is approximately 2.4 V, differing by 1 V from the 3.5 V estimated by David et al.[18] Nevertheless, our calculations still support the instability of Bk(V). The Cf(V/IV) potential was extremely positive, ca. 3.4 V, indicating a consistent trend across these elements.

For the An^{+m}/An(0) redox potentials, some are available experimentally.[2,85−92] Such potentials were determined through radiopolarography techniques combined with estimated amalgamation energies. The amalgamation energies are

Table 7. Reduction Potentials E° for Ac to Lr in Different Oxidation States in Aqueous Solution (Potentials in Volts Relative to SHE; Values Obtained at the B3LYP/ECP(60)/TZVP//COSMO Level Unless Indicated)

Potential	Ac	Th	Pa	U	Np	Pu	Am	Cm	Bk	Cf	Es	Fm	Md	No	Lr
I/0	−0.62	1.94	1.58	1.55	2.64	1.77	0.75	0.51	1.20	3.81	−1.27	−0.18	−0.06	0.07	
II/0	−1.45	−0.06	−0.55	−0.64	−0.55	−1.13	−1.39	−0.79	−1.49[c]	−2.18[c]	−2.25	−2.27[c]	−2.53[c]	−2.37[c]	−1.51[c]
III/0	−2.09	−1.13	−1.51	−1.53	−1.95	−1.84	−1.93	−2.12[c]	−1.85	−1.97[c]	−2.04	−1.95[c]	−1.70	−1.35[c]	−2.09[c]
IV/0		−1.68	−1.74	−1.52	−1.37	−1.32	−1.03	−0.68	−1.16	−0.79[c]					
II/I	−2.23	−2.01	−2.55	−2.60	−3.51	−4.09	−3.06	−2.25	−3.14	−3.10	−3.22	−3.19	−3.29	−3.35	
III/II	−3.05	−3.38	−2.96	−2.97	−2.98	−1.58	−1.13	−2.86	−2.32[c]	−1.66[d]	−1.44[d]	−1.14[e]	−0.08[d]	1.42[c]	−2.93
IV/III		−2.26	−1.59	−0.29	0.58	1.48	2.76	3.13	1.68[c]	2.89	3.72				
V/III				−0.09	0.48	1.02	1.81	2.84	2.13	3.05					
V/IV			−0.31[a]	0.11	0.39	0.57	0.87	2.55	2.30	3.76					
VI/III				0.00	0.66	1.27	1.81	2.68							
VI/IV				0.15	0.71	1.17	1.34	2.46							
VI/V				0.18	1.02	0.89[b]	1.81	2.20							
VII/VI					2.72	2.78	3.01								

[a]$Pa(V)OOH^{+2}/Pa^{4+}$. [b]PW91/ECP(60)/TZVP//COSMO. [c]B3LYP/ECP(60)/TZVP//SMD. [d]B3LYP/ECP(60)/TZVP//COSMO + SO. [e]B3LYP/ECP(60)/TZVP//SMD + SO.

estimated using the metal radii as a correlating parameter, with interpolation performed within a series of divalent elements possessing known amalgamation potentials.[93] Hulet[94] cautions against relying heavily on this correction, as the amalgamation potential constitutes a substantial amount in the determination of standard redox potentials, especially for the latter actinides. Our computational approach depends on the use of I.E. values, so a range of energy values were tested. The later actinides have fewer available experimental I.E. values compared to the earlier elements in the series, with data typically limited to only the first ionization energy.[95−100] Most of the higher I.E. values are determined by extrapolation methods or high-level quantum chemistry methods. The different sets used are given in the SI. Depending on the actinide, these energies can significantly differ from one another. In our previous work, the $An^{+m}/An(0)$ potentials showed better agreement with experiments when considering the COSMO solvation model.[19,20] Our calculated An(III/0) values agreed with the experimental data, with the current set of ionization energies employed, especially with the COSMO solvation model. For An(III/0), the best agreement was obtained using the NIST recommended values. Specifically, the deviations from experimental An(III/0) redox values were as follows: +0.19 V for Cm(III/0),[85] +0.15 V for Bk(III/0),[86] −0.18 V for Cf(III/0),[87] −0.25 V for Es(III/0),[88] −0.20 V for Fm(III/0),[89] +0.04 V for Md(III/0),[90] +0.17 V for No(III/0),[90] and +0.32 V for Lr(III/0).[92]

The calculated An(II/0) potentials all displayed negative values, indicating the preference for the divalent oxidation state in solution, rather than the metallic state. Comparing the An(II/0) potentials with the experimental data for Md[2] and No,[91] the COSMO calculations differ significantly, no matter which set of I.E. values was used. For An(II/0), the COSMO values were less negative than previous estimates[17] for Cm, Bk, Cf, Md, and Lr and the SMD values were more negative. For Es, both solvent approaches predicted more negative values than prior estimates,[17] whereas for No, both methods predicted less negative values. The An(II/0) potentials predicted with SMD were in general closer to prior estimates.[17] For the An(IV/0) potentials, estimates[17] are available for Cm, Bk, and Cf, and the best agreement is found using COSMO with the set (iii) I.E. values.

Spin−Orbit Effects. As in previous studies,[19−21] we also examined the spin−orbit effects on ionization energies, with the results presented in Table 5. Comparing bare and solvated ions, the spin−orbit effects have a significantly greater impact on ionization energies for bare ions than for solvated systems. However, as we move across the series, starting from Es, the spin−orbit effects increase even in solvated systems. This trend also coincides with the fact that these later actinides exhibit the largest discrepancies between computed potentials and experimental data or estimates. Even though the late actinides have fewer unpaired electrons than their predecessors, their electronic structures remain extremely challenging to model. This complexity arises from a combination of relativistic effects, multireference character, and strong electron correlation. The calculated SO effects can be used to improve estimates of the redox potentials, as shown in Table 6. Up to Cf, the redox potentials showed minimal variation upon inclusion of spin−orbit corrections. For heavier elements such as Md, No, and Lr, especially in redox pairs

involving high oxidation states, the SO can impact the values. For An(II/(I) pairs, the effects are generally small. For the III/II potentials,

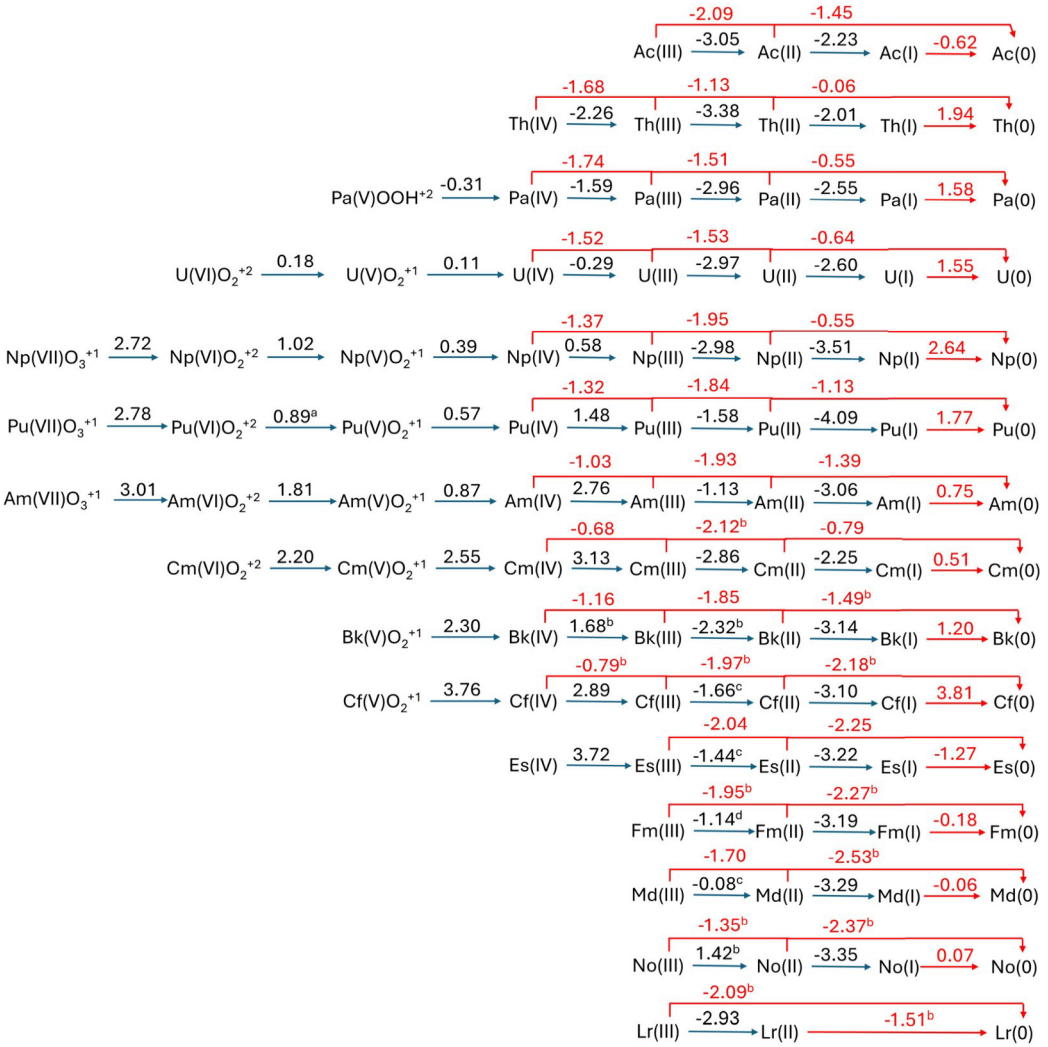

Figure 4. Latimer diagram for reduction potentials E° for Ac to Lr in different oxidation states in aqueous solution. Potentials in volts relative to SHE. Values obtained at the B3LYP/ECP(60)/TZVP//COSMO level unless indicated by superscript labels. (a) PW91/ECP(60)/TZVP// COSMO. (b) B3LYP/ECP(60)/TZVP//SMD. (c) B3LYP/ECP(60)/TZVP//COSMO + SO. (d) B3LYP/ECP(60)/TZVP//SMD + SO.

the inclusion of SO corrections improved agreement with experimental data. The Cf(III/II), Es(III/II), Fm(III/II) (SMD level), and Md(III/II) couples have more negative redox potentials and show better agreement with the experimental data.

Trends in Calculated Redox Potentials. We now describe the trends in the calculated redox potentials in acidic media from Ac to Lr for multiple oxidation states including our prior work.[19,20] The results in best agreement with experimental or estimated data are presented in Table 7; most of the results were obtained at the B3LYP/ECP(60)/ TZVP//COSMO level unless indicated. A Latimer diagram is given in Figure 4 with An^{+m}/An(0) redox processes in red. The B3LYP functional in combination with the Stuttgart ECP60 pseudopotential for actinides, and TZVP basis for H and O atoms proved to be an appropriate level of theory for calculating redox potentials in aqueous solution. An exception is the Pu(VI/V) couple, where the PW91 functional provided a value closer to the experimental potential. From Ac to Cm, the COSMO solvation model provided the best results, whereas starting from Bk, some calculated potentials agreed better when using SMD solvation model. Although some An(III/II) potentials are improved with inclusion of spin−orbit corrections, inclusion of only scalar relativistic effects provided reasonable agreement with literature values.

For the reduction to the metallic state, both the An(I/0) and An(II/0) couples are highly negative across the series, indicating that deposition of the bulk metal from aqueous solution is thermodynamically unfavorable. The An(II/I) and An(III/II) couples show that the +I state is strongly disfavored, with potentials around −2.0 to −4.0 V, whereas

stabilization of the +II state becomes possible starting at Pu. There is no complete set of available experimental data for the An(II/I), An(V/IV), and An(VI/V) couples across the actinide series, which makes direct comparison difficult. Nevertheless, the calculated values provide valuable insight into their relative stabilities.

The calculated redox potentials from Ac to Lr reveal clear systematic trends across the series that align well with experimental expectations. Our calculated values indicate that from Pa to Pu the higher oxidation states (+IV, +V, +VI), reduction potentials are moderately negative to slightly positive. Pa exhibits a unique stability in the +V state, as reflected in its accessible Pa(V)/Pa(IV) potential, whereas the most stable Pa(V) form is the protonated $Pa(V)OOH^{+2}$.[101] The highest oxidation states, accessed through the An(VI/V) and An(VII/VI) couples, are limited to U, Np, and Pu. The middle of the series (Am-Cm) show a crossover behavior where +III becomes the most stable oxidation state, as indicated by the strongly positive An(IV/III) potentials. The late actinides are dominated by +III oxidation state. However, the calculated reduction potentials for the divalent states of Md and No, which range from moderately negative to slightly positive values, suggest that these oxidation states can indeed be accessed under suitable conditions.

CONCLUSIONS

We extended our computational methodology[19−21] to predict standard redox potentials in aqueous acidic solutions for Cm, Bk, Cf, Es, Fm, Md, No, and Lr for a range of oxidation states. Our approach is based on using B3LYP/ECP(60)/explicit H_2O/SCRF scalar relativistic approach to estimate the redox potentials. Due to the instability and scarcity of these elements, there are few reliable experimental data. The hydration number and averaged metal-water bond distances were consistent with available experimental data for the few elements, Cm(III), Bk(III), Bk(IV), and Cf(III), with measurements.[70,76−80] Overall, our results are consistent with prior computational studies, except for the Cm(IV) ion.[64−67,81,82] In general, our approach can predict An(III/II) redox potentials within a margin of ±0.2 V of the available experimental data for most of the couples. However, no single solvation model provided completely satisfactory results, as SMD showed better agreement than COSMO in certain cases. There is no available experimental data for the An(II/I), An(V/IV), and An(VI/V) potentials for these elements. Although some of the estimated values do not match our more reliable calculated results numerically, they exhibit a similar trend to what we predicted for the relative stability of specific oxidation states.

The $An^{+m}/An(0)$ redox potentials are predicted using a Born−Haber cycle, which includes sublimation and ionization energies available in the literature, and our calculated hydration energies. Due to a lack of experimental ionization energies for some oxidation states, three different sets of ionization energies were used, taken from selected combinations of available experimental data and computational studies.[2,85−92] The redox potentials depend on the choice of I.E.s. Unlike previous studies,[19,20] which found the best agreement with experimental data exclusively when using the COSMO solvation model, our calculations for $An^{+m}/An(0)$ redox potentials showed that SMD also yielded satisfactory results for selected redox couples. The An(III/0) potentials show better agreement with experiment with the COSMO solvation models and the I.E. values from the NIST database. In general, the differences between the calculated values and experiment were around ±0.2 V for most redox couples. However, for the Md(II/0) couple, SMD provided better results. For No(II/0), no solvation model or set of ionization energies predicts a result consistent with the reported experimental value. Our spin− orbit calculations indicate a quenching effect on the redox potential prediction for most solvated systems. Starting from Es, some cations still retain a significant spin−orbit coupling contribution in solution. These coincide with the result that the calculated redox potentials for these elements deviated the most from experiment. Inclusion of spin−orbit effects can improve the predicted redox potentials, particularly for those involving higher oxidation states of the heavier actinides. Even with the limitations of the available experimental data, our computational methods were able to predict redox potentials in reasonable agreement with the current most accepted values for most redox couples.

ASSOCIATED CONTENT

* Supporting Information

The Supporting Information is available free of charge at https://pubs.acs.org/doi/10.1021/acs.jpca.5c06523.

Complete references 3, 34, 48, 82, 84, 96−100; ionization energies used; energies (a.u.) of each actinide cluster in the gas and aqueous phases; and optimized geometries in Cartesian (x, y, z) coordinates in Å (PDF)

AUTHOR INFORMATION

Corresponding Author

David A. Dixon − *Department of Chemistry and Biochemistry, The University of Alabama, Tuscaloosa, Alabama 35487, United States;* orcid.org/0000-0002-9492-0056; Email: dadixon@ua.edu

Author

Felipe R. Dutra − *Instituto de Química, Universidade Estadual de Campinas, 13083-970 Campinas, São Paulo, Brazil; Department of Chemistry and Biochemistry, The University of Alabama, Tuscaloosa, Alabama 35487, United States*

Complete contact information is available at: https://pubs.acs.org/10.1021/acs.jpca.5c06523

Notes

The authors declare no competing financial interest.

ACKNOWLEDGMENTS

This work was supported by the U.S. Department of Energy (DOE), Office of Science, Office of Basic Energy Sciences, Heavy Element Chemistry Program at The University of Alabama (D.A.D.) through Grant No. DE-SC0018921. F.R.D. expresses gratitude for the scholarship provided by grant 2023/ 02596-0, São Paulo Research Foundation (FAPESP). D.A.D. thanks the Robert Ramsay and the Endowed Shelby Distinguished Professor Funds at The University of Alabama for support.

REFERENCES

(1) Mikheev, V. B.; Spitsyn, V. I.; Ionova, G. V.; Auerman, l. N. The Stabilities of the Oxidation States of the Lanthanides and Actinides. *Radiochim. Acta* 1984, *37*, 181−186.

(2) Edelstein, N. M.; Fuger, J.; Katz, J. J.; Morse, L. R. Summary and Comparison of Properties of the Actinide and Transactinide Elements. In *The Chemistry of the Actinide and Transactinide Elements*; Morss, L. R., Edelstein, N. M., Fuger, J., Eds.; Springer Netherlands, Dordrecht, 2011; pp 1753−1835.

(3) Pore, J. L.; Gates, J. M.; Dixon, D. A.; Garcia, F. H.; Gibson, J. K.; Gooding, J. A.; McCarthy, M.; Orford, R.; Shafi, Z.; Shuh, D. K.; Sprouse, S. Atom-at-a-Time Actinium and Nobelium Coordination Chemistry: A Comparison of Directly Identified Molecular Species Produced in Gas Phase Reactions. *Nature* 2025, *644*, 376−380.

(4) Choppin, G. R. Solution Chemistry of the Actinides. *Radiochim. Acta* 1983, *32*, 43−54.

(5) Kosyakov, V. N.; Timofeev, G. A.; Erin, E. A.; Andreev, V. I.; Kopytov, V. V.; Simakin, G. A. Preparation and Stability of Americium (4), Curium (4) and Californium (4) in Potassium Phosphotungstate Solutions. *Radiokhimiya* 1977, *19* (4), 511−517.

(6) Hobart, D. E.; Varlashkin, P. G.; Samhoun, K.; Haire, R. G.; Peterson, J. R. Spectroscopic and Redox Properties of Curium and Californium Ions in Concentrated Aqueous Carbonate-Bicarbonate Media. *Rev. Chim. Miner.* 1983, *20*, 817−827.

(7) Kovács, A.; Dau, P. D.; Marçalo, J.; Gibson, J. K. Pentavalent Curium, Berkelium, and Californium in Nitrate Complexes: Extending Actinide Chemistry and Oxidation States. *Inorg. Chem.* 2018, *57*, 9453−9467.

(8) Spitsyn, V. I.; Ionova, G. V. Higher States of Curium Oxidation. *Radiokhimiya.* 1978, *20* (3), 328−332.

(9) Domanov, V. P.; Lobanov, Yu. V. Formation of Volatile Curium(VI) Trioxide CmO_3. *Radiochemistry* 2011, *53*, 453−456.

(10) Domanov, V. P. Possibility of Generation of Octavalent Curium in the Gas Phase in the Form of Volatile Tetraoxide CmO_4. *Radiochemistry* 2013, *55*, 46−51.

(11) Mikheev, N. B.; Spitsyn, V. I.; Kamenskaya, A. N.; Rumer, I. A.; Gvozdev, B. A.; Rozenkevich, N. A.; Auehrman, L. N. Mendelevium Reduction to the Monovalent State. *Doklady Akademii Nauk SSSR, Seriya Fizicheskoj Khimii* 1973, *208*, 1146−1149.

(12) Samhoun, K.; David, F.; Hahn, R. L.; O'Kelley, G. D.; Tarrant, J. R.; Hobart, D. E. Electrochemical Study of Mendelevium in Aqueous Solution: No Evidence for Monovalent Ions. *J. Inorg. Nucl. Chem.* 1979, *41*, 1749−1754.

(13) Hulet, E. K.; Lougheed, R. W.; Baisden, P. A.; Landrum, J. H.; Wild, J. F.; Lundqvist, R. F. D. Non-Observance of Monovalent Md. *J. Inorg. Nucl. Chem.* 1979, *41*, 1743−1747.

(14) Scherer, U.; Kratz, J.; Schädel, M.; Brüchle, W.; Gregorich, K. E.; Henderson, R.; Lee, D.; Nurmia, M.; Hoffman, D. Lawrencium Chemistry: No Evidence for Oxidation States Lower than 3+ in Aqueous Solution. *Inorg. Chim. Acta* 1988, *146*, 249−254.

(15) David, F.; Ionova, G.; Guillaumont, R. E° (3/2) Redox Potentials of Lanthanides and Actinides with F^qd Electronic Configuration. *J. Radioanal. Nucl. Chem.* 1995, *199*, 35−40.

(16) Nugent, L. J.; Baybarz, R. D.; Burnett, J. L.; Ryan, J. L. ElectronTransfer and f-d Absorption Bands of Some Lanthanide and Actinide Complexes and the Standard (II-III) Oxidation Potential for Each Member of the Lanthanide and Actinide Series. *J. Phys. Chem.* 1973, *77*, 1528−1539.

(17) Bratsch, S. G.; Lagowski, J. J. Actinide Thermodynamic Predictions. 3. Thermodynamics of Compounds and Aquo-Ions of the 2+, 3+, and 4+ Oxidation States and Standard Electrode Potentials at 298.15 K. *J. Phys. Chem.* 1986, *90*, 307−312.

(18) David, F.; Samhoun, K.; Guillaumont, R.; Nugent, L. J. Heavy Element Properties. In *Proceedings of the Joint Session, 4th International Transplutonium Element Symposium & 5th International Conference on Plutonium and Other Actinides, Baden-Baden, September 1975*; Müller, W., Blank, H., Eds.; North-Holland, Amsterdam, 1976; pp 97−104.

(19) Dutra, F. R.; Romeu, J. G. F.; Dixon, D. A. Prediction of Redox Potentials for Ac, Th, and Pa in Aqueous Solution. *J. Phys. Chem. A* 2024, *128*, 9730−9746.

(20) Dutra, F. R.; Vasiliu, M.; Gomez, A. N.; Xia, D.; Dixon, D. A. Prediction of Redox Potentials for U, Np, Pu, and Am in Aqueous Solution. *J. Phys. Chem. A* 2024, *128*, 5612−5626.

(21) Dutra, F. R.; Dixon, D. A. Prediction of Redox Potentials for Different Oxidation States of U, Np, Pu, and Am in Alkaline Aqueous Solution. *J. Phys. Chem. A* 2025, *129*, 2521−2536.

(22) Klamt, A.; Schüürmann, G. COSMO: A New Approach to Dielectric Screening in Solvents with Explicit Expressions for the Screening Energy and Its Gradient. *J. Chem. Soc., Perkin Trans.* 1993, *2* (5), 799−805.

(23) Klamt, A. In *COSMO-RS: From Quantum Chemistry to Fluid Phase Thermodynamics and Drug Design*; Elsevier, Amsterdam, 2005.

(24) Marenich, A. V.; Cramer, C. J.; Truhlar, D. G. Universal Solvation Model Based on Solute Electron Density and on a Continuum Model of the Solvent Defined by the Bulk Dielectric Constant and Atomic Surface Tensions. *J. Phys. Chem. B* 2009, *113*, 6378−6396.

(25) Tomasi, J.; Mennucci, B.; Cammi, R. Quantum Mechanical Continuum Solvation Models. *Chem. Rev.* 2005, *105*, 2999−309.

(26) Marenich, A. V.; Ho, J.; Coote, M. L.; Cramer, C. J.; Truhlar, D. G. Computational Electrochemistry: Prediction of Liquid-Phase Reduction Potentials. *Phys. Chem. Chem. Phys.* 2014, *16*, 15068−15106.

(27) Zhan, C. G.; Dixon, D. A. Absolute Hydration Free Energy of the Proton from First-Principles Electronic Structure Calculations. *J. Phys. Chem. A* 2001, *105*, 11534−11540.

(28) Feng, R.; Vasiliu, M.; Peterson, K. A.; Dixon, D. A. Acidity of $M(VI)O_2(OH)_2$ for M = Group 6, 16, and U as Central Atoms. *J. Phys. Chem. A* 2017, *121*, 1041−1050.

(29) Lee, Z. R.; Quinn, L. J.; Jones, C. W.; Hayes, S. E.; Dixon, D. A. Predicting the Mechanism and Products of CO_2 Capture by Amines in the Presence of H_2O. *J. Phys. Chem. A* 2021, *125*, 9802−9818.

(30) Gutowski, K. E.; Dixon, D. A. Ab Initio Prediction of the Gasand Solution-Phase Acidities of Strong Brønsted Acids: The Calculation of PKa Values Less Than−10. *J. Phys. Chem. A* 2006, *110*, 12044−12054.

(31) Parr, R. G.; Yang, W. In *Density-Functional Theory of Atoms and Molecules*; Oxford University Press, New York, 1989.

(32) Becke, A. D. Density-functional Thermochemistry. III. The Role of Exact Exchange. *J. Chem. Phys.* 1993, *98*, 5648−5652.

(33) Lee, C.; Yang, W.; Parr, R. G. Development of the ColleSalvetti Correlation-Energy Formula into a Functional of the Electron Density. *Phys. Rev. B* 1988, *37*, 785−789.

(34) Frisch, M. J.; Trucks, G. W.; Schlegel, H. B.; Scuseria, G. E.; Robb, M. A.; Cheeseman, J. R.; Scalmani, G.; Barone, V.; Petersson, G. A.; Nakatsuji, H.; et al. *Gaussian 16, Revision A.03*; Gaussian, Inc., Wallingford, CT, 2016.

(35) Godbout, N.; Salahub, D. R.; Andzelm, J.; Wimmer, E. Optimization of Gaussian-type Basis Sets for Local Spin Density Functional Calculations. Part I. Boron Through Neon, Optimization Technique and Validation. *Can. J. Chem.* 1992, *70*, 560−571.

(36) Peterson, K. Correlation Consistent Basis Sets for Actinides. I. The Th and U Atoms. *J. Chem. Phys.* 2015, *142*, No. 074105.

(37) Kuchle, W.; Dolg, M.; Stoll, H.; Preuss, H. Energy-Adjusted Pseudopotentials for the Actinides. Parameter sets and Test Calculations for Thorium and Thorium Monoxide. *J. Chem. Phys.* 1994, *100*, 7535−7542.

(38) Cao, X.; Dolg, M. Segmented Contraction Scheme for SmallCore Actinide Pseudopotential Basis sets. *J. Mol. Struc. - THEOCHEM* 2004, *673*, 203−209.

(39) Cao, X.; Dolg, M.; Stoll, H. Valence Basis Sets for Relativistic Energy-Consistent Small-Core Actinide Pseudopotentials. *J. Chem. Phys.* 2003, *118*, 487−496.

(40) Luchini, G.; Alegre-Requena, J. V.; Funes-Ardoiz, I.; Paton, R. S. GoodVibes: Automated Thermochemistry for Heterogeneous Computational Chemistry Data [Version 1; Peer Review: 2 Approved with Reservations]. *F1000Res.* 2020, *9*, 291.

(41) Ribeiro, R. F.; Marenich, A. V.; Cramer, C. J.; Truhlar, D. G. Use of Solution-Phase Vibrational Frequencies in Continuum Models for the Free Energy of Solvation. *J. Phys. Chem. B* 2011, *115*, 14556− 14562.

(42) Shimodaira, Y.; Miura, T.; Kudo, A.; Kobayashi, H. DFT Method Estimation of Standard Redox Potential of Metal Ions and Metal Complexes. *J. Chem. Theory. Comput.* 2007, *3*, 789−795.

(43) Funes-Ardoiz, I.; Maseras, F. On the Use of Thermodynamic Cycles for the Calculation of Standard Potentials for the Oxidation of Solid Metals in Solution. *ChemPhysChem* 2019, *20*, 159−162.

(44) Konings, R. J. M.; Morss, L. R.; Fuger, J. Thermodynamic Properties of Actinides and Actinide Compounds. In *The Chemistry of the Actinide and Transactinide Elements*; Morss, L. R., Edelstein, N. M., Fuger, J., Eds.; Springer Netherlands, Dordrecht, 2011; pp 2113− 2224.

(45) Feng, R.; Peterson, K. Correlation Consistent Basis Sets for Actinides. II. The Atoms Ac and Np−Lr. *J. Chem. Phys.* 2017, *147*, 084108.

(46) Pantazis, D. A.; Neese, F. All-Electron Scalar Relativistic Basis Sets for the Actinides. *J. Chem. Theory Comput.* 2011, *7*, 677−684.

(47) te Velde, G.; Bickelhaupt, F. M.; van Gisbergen, S. J. A.; Fonseca Guerra, C.; Baerends, E. J.; Snijders, J. G.; Ziegler, T. Chemistry with ADF. *J. Comput. Chem.* 2001, *22*, 931−967.

(48) Baerends, E. J.; Aguirre, N. F.; Austin, N. D.; Autschbach, J.; Bickelhaupt, F. M.; Bulo, R.; Cappelli, C.; van Duin, A. C. T.; Egidi, F.; Fonseca Guerra, C.; et al. The Amsterdam Modeling Suite. *J. Chem. Phys.* 2025, *162*, 162501.

(49) van Lenthe, E.; Ehlers, A. E.; Baerends, E. J. Geometry Optimization in the Zero Order Regular Approximation for Relativistic Effects. *J. Chem. Phys.* 1999, *110*, 8943−8953.

(50) Lenthe, E. v.; Baerends, E. J.; Snijders, J. G. Relativistic Regular
Two-Component Hamiltonians. *J. Chem. Phys.* 1993, *99*, 4597−4610.

(51) van Lenthe, E.; Baerends, E. J.; Snijders, J. G. Relativistic Total Energy Using Regular Approximations. *J. Chem. Phys.* 1994, *101*, 9783−9792.

(52) van Lenthe, E.; Snijders, J. G.; Baerends, E. J. The Zero-Order Regular Approximation for Relativistic Effects: The Effect of SpinOrbit Coupling in Closed Shell Molecules. *J. Chem. Phys.* 1996, *105*, 6505−6516.

(53) van Lenthe, E.; van Leeuwen, R.; Baerends, E. J.; Snijders, J. G. Relativistic Regular Two-Component Hamiltonians. *Int. J. Quantum Chem.* 1996, *57*, 281−293.

(54) Becke, A. D. Density-Functional Exchange-Energy Approximation with Correct Asymptotic Behavior. *Phys. Rev. A* 1988, *38*, 3098−3100.

(55) Lee, C.; Yang, W.; Parr, R. G. Development of the ColleSalvetti Conelation Energy Formula into a Functional of the Electron Density. *Phys. Rev. B* 1988, *37*, 785−789.

(56) Cheng, J.; Liu, X.; VandeVondele, J.; Sulpizi, M.; Sprik, M. Redox Potentials and Acidity Constants from Density Functional Theory Based Molecular Dynamics. *Acc. Chem. Res.* 2014, *47*, 3522− 3529.

(57) Liu, X.; Cheng, J.; Sprik, M. Aqueous Transition-Metal Cations as Impurities in a Wide Gap Oxide: The Cu^{2+}/Cu^{+} and Ag^{2+}/Ag^{+} Redox Couples Revisited. *J. Phys. Chem. B* 2015, *119*, 1152−1163.

(58) McNeill, A. S.; Dixon, D. A. Energetics of CO_2^- in Aqueous Solution. *J. Phys. Chem. A* 2019, *123*, 1243−1259.

(59) McNeill, A. S.; Zhan, C.-G.; Appel, A. M.; Stanbury, D. M.; Dixon, D. A. The $H^{\bullet}/H^-$ Redox Couple and Absolute Hydration Energy of H. *J. Phys. Chem. A* 2020, *124*, 6084−6095.

(60) Andress, T. D.; Maxwell, J. W.; McNeill, A. S.; Stanbury, D. M.; Dixon, D. A. Prediction of Aqueous Reduction Potentials of $X^{\bullet}$, $ChH^{\bullet}$, and $XO^{\bullet}$ Radicals with X = Halogen and Ch = Chalcogen. *J. Phys. Chem. A* 2023, *127*, 10600−10612.

(61) Andress, T. D.; Stanbury, D. M.; Dixon, D. A. Calculated Aqueous Reduction Potentials of Neutral and Anionic Halogen Diatomic Molecules. *J. Phys. Chem. A* 2024, *128*, 6494−6509.

(62) David, F.; Fourest, B.; Duplessis, J. Hydration Thermodynamics of Plutonium and Transplutonium Ions. *J. Nucl. Mater.* 1985, *130*, 273−279.

(63) David, F. About Low Oxidation States, Hydration and Covalence Properties of f Elements. *Radiochim. Acta* 2008, *96*, 135−144.

(64) Watanabe, E.; Nakajima, T.; Shinohara, A.; Kasamatsu, Y. Hydration Structure of $_{102}No^{2+}$: A Density Functional TheoryMolecular Dynamics Study. *J. Phys. Chem. A* 2024, *128*, 2717−2726. (65) D'Angelo, P.; Martelli, F.; Spezia, R.; Filipponi, A.; Denecke, M. A. Hydration Properties and Ionic Radii of Actinide(III) Ions in Aqueous Solution. *Inorg. Chem.* 2013, *52*, 10318−10324.

(66) Duvail, M.; Martelli, F.; Vitorge, P.; Spezia, R. Polarizable Interaction Potential for Molecular Dynamics Simulations of Actinoids(III) in Liquid Water. *J. Chem. Phys.* 2011, *135*, 044503.

(67) Wiebke, J.; Moritz, A.; Cao, X.; Dolg, M. Approaching Actinide(+III) Hydration from First Principles. *Phys. Chem. Chem. Phys.* 2007, *9*, 459−465.

(68) Kimura, T.; Choppin, G. R. Luminescence Study on Determination of the Hydration Number of Cm(III). *J. Alloys Compd.* 1994, *213−214*, 313−317.

(69) Kimura, T.; Choppin, G. R.; Kato, Y.; Yoshida, Z. Determination of the Hydration Number of Cm (III) in Various Aqueous Solutions. *Radiochim. Acta* 1996, *72*, 61−64.

(70) Allen, P. G.; Bucher, J. J.; Shuh, D. K.; Edelstein, N. M.; Craig, I. Coordination Chemistry of Trivalent Lanthanide and Actinide Ions in Dilute and Concentrated Chloride Solutions. *Inorg. Chem.* 2000, *39*, 595−601.

(71) Stumpf, T.; Fanghänel, T.; Grenthe, I. Complexation of Trivalent Actinide and Lanthanide Ions by Glycolic Acid: A TRLFS Study. *J. Chem. Soc., Dalton Trans.* 2002, *20*, 3799−3804.

(72) Lindqvist-Reis, P.; Klenze, R.; Schubert, G.; Fanghänel, T. Hydration of Cm^{3+} in Aqueous Solution from 20 to 200 °C. A TimeResolved Laser Fluorescence Spectroscopy Study. *J. Phys. Chem. B* 2005, *109*, 3077−3083.

(73) Yang; Bursten, B. E. Speciation of the Curium(III) Ion in Aqueous Solution: A Combined Study by Quantum Chemistry and Molecular Dynamics Simulation. *Inorg. Chem.* 2006, *45*, 5291−5301.

(74) Hagberg, D.; Bednarz, E.; Edelstein, N. M.; Gagliardi, L. A Quantum Chemical and Molecular Dynamics Study of the Coordination of Cm(III) in Water. *J. Am. Chem. Soc.* 2007, *129*, 14136−14137.

(75) Atta-Fynn, R.; Bylaska, E. J.; Schenter, G. K.; de Jong, W. A. Hydration Shell Structure and Dynamics of Curium(III) in Aqueous Solution: First Principles and Empirical Studies. *J. Phys. Chem. A* 2011, *115*, 4665−4677.

(76) Lindqvist-Reis, P.; Apostolidis, C.; Rebizant, J.; Morgenstern, A.; Klenze, R.; Walter, O.; Fanghänel, T.; Haire, R. G. The Structures and Optical Spectra of Hydrated Transplutonium Ions in the Solid State and in Solution. *Angew. Chem., Int. Ed.* 2007, *46*, 919−922.

(77) Skanthakumar, S.; Antonio, M. R.; Wilson, R. E.; Soderholm, L. The Curium Aqua Ion. *Inorg. Chem.* 2007, *46*, 3485−3491.

(78) Antonio, M. R.; Williams, C. W.; Soderholm, L. Berkelium Redox Speciation. *Radiochim. Acta* 2002, *90*, 851−856.

(79) Revel, R.; den Auwer, C.; Madic, C.; David, F.; Fourest, B.; Hubert, S.; Le Du, J.-F.; Morss, L. R. First Investigation on the L Edges of the ^{249}Cf Aquo Ion by X-Ray Absorption Spectroscopy. *Inorg. Chem.* 1999, *38*, 4139−4141.

(80) Galbis, E.; Hernández-Cobos, J.; den Auwer, C.; Le Naour, C.; Guillaumont, D.; Simoni, E.; Pappalardo, R. R.; Sánchez Marcos, E. Solving the Hydration Structure of the Heaviest Actinide Aqua Ion Known: The Californium(III) Case. *Angew. Chem.* 2010, *49*, 3811− 3815.

(81) Acher, E.; Masella, M.; Vallet, V.; Réal, F. Properties of the Tetravalent Actinide Series in Aqueous Phase from a Microscopic Simulation Self-Consistent Engine. *Phys. Chem. Chem. Phys.* 2020, *22*, 2343−2350.

(82) Banik, N. L.; Vallet, V.; Réal, F.; Belmecheri, R. M.; Schimmelpfennig, B.; Rothe, J.; Marsac, R.; Lindqvist-Reis, P.; Walther, C.; Denecke, M. A.; et al. First Structural Characterization of Pa(IV) in Aqueous Solution and Quantum Chemical Investigations of the Tetravalent Actinides up to Bk(IV): The Evidence of a Curium Break. *Dalton Trans.* 2016, *45*, 453−457.

(83) Mikheev, N. B.; Auerman, L. N.; Rumer, I. A.; Kamenskaya, A. N.; Kazakevich, M. Z. The Anomalous Stabilisation of the Oxidation State 2+ of Lanthanides and Actinides. *Russ. Chem. Rev.* 1992, *61*, 990−998.

(84) Toyoshima, A.; Li, Z.; Asai, M.; Sato, N.; Sato, T. K.; Kikuchi, T.; Kaneya, Y.; Kitatsuji, Y.; Tsukada, K.; Nagame, Y.; et al. Measurement of the Md^{3+}/Md^{2+} Reduction Potential Studied with Flow Electrolytic Chromatography. *Inorg. Chem.* 2013, *52*, 12311−12313.

(85) Fuger, J.; Reul, J.; Muller, W. A New Determination of the Enthalpy of Solution of Curium Metal and the Enthalpies of Formation of Cm^{3+}(aq) and $CmCl_3$(s). *Inorg. Nucl. Chem. Lett.* 1975, *11*, 265−275.

(86) Fuger, J.; Haire, R. G.; Peterson, J. R. A New Determination of the Enthalpy of Solution of Berkelium Metal and

the Standard Enthalpy of Formation of Bk^{3+}(aq). *J. Inorg. Nucl. Chem.* 1981, *43*, 3209−3212.

(87) Fuger, J.; Haire, R. G.; Peterson, J. R. The Enthalpy of Solution of Californium Metal and the Standard Enthalpy of Formation of Cf^{3+}(aq). *J. L. Comm. Met.* 1984, *98*, 315−321.

(88) Samhoun, K.; David, F. Electrochemical Reduction by Radiopolarography of Some Transplutonium Aqueous Ions. *J. Inorg. Nucl. Chem.* 1979, *41*, 357−363.

(89) Morss, L. R. Thermodynamic Systematics of Oxides of Americium, Curium, and Neighboring Elements. In *Americium and Curium Chemistry and Technology: Papers from a Symposium given at the 1984 International Chemical Congress of Pacific Basin Societies, Honolulu, HI, December 16–27, 1984*; Norman, E. M., Navratil, J. D., Schulz, W. W., Eds.; Springer Netherlands, Dordrecht, 1985; pp 147− 158.

(90) David, F. Oxidation Reduction and Thermodynamic Properties of Curium and Heavier Actinide Elements. In *Handbook of the Physics and Chemistry of the Actinides*; Freeman, A. J., Keller, C., Eds.; Elsevier, 1986; pp 97−128.

(91) Meyer, R. E.; McDowell, W. J.; Dittner, P. F.; Silva, R. J.; Tarrant, J. R. Determination of the Half-Wave Potential of Nobelium. *J. Inorg. Nucl. Chem.* 1976, *38*, 1171−1173.

(92) David, F.; Samhoun, K.; Guillaumont, R.; Edelstein, N. Thermodynamic Properties of 5f Elements. *J. Inorg. Nucl. Chem.* 1978, *40*, 69−74.

(93) Nugent, L. J. Standard Electrode Potentials and Enthalpies of Formation of Some Lanthanide and Actinide Aquo-Ions. *Journal of Inorganic and Nuclear Chemistry* 1975, *37*, 1767−1770.

(94) Hulet, E. K. Chemistry of the Heaviest Actinides: Fermium, Mendelevium, Nobelium, and Lawrencium. In *Lanthanide and Actinide Chemistry and Spectroscopy*; ACS Symposium Series, Vol. *131*; American Chemical Society, 1980; pp 239−263.

(95) Kneip, N.; Weber, F.; Kaja, M. A.; Düllmann, C. E.; Mokry, C.; Raeder, S.; Runke, J.; Studer, D.; Trautmann, N.; Wendt, K. Investigation of the Atomic Structure of Curium and Determination of Its First Ionization Potential. *European Physical Journal D* 2022, *76*, 190.

(96) Köhler, S.; Deißenberger, R.; Eberhardt, K.; Erdmann, N.; Herrmann, G.; Huber, G.; Kratz, J. V.; Nunnemann, M.; Passler, G.; Rao, P. M.; et al. Determination of the First Ionization Potential of Actinide Elements by Resonance Ionization Mass Spectroscopy. *Spectrochim. Acta Par. B At Spectrosc.* 1997, *52*, 717−726.

(97) Weber, F.; Düllmann, C. E.; Gadelshin, V.; Kneip, N.; Oberstedt, S.; Raeder, S.; Runke, J.; Mokry, C.; Thörle-Pospiech, P.; Studer, D.; et al. Probing the Atomic Structure of Californium by Resonance Ionization Spectroscopy. *Atoms* 2022, *10*, 51.

(98) Weber, F.; Albrecht-Schönzart, T. E.; Block, M.; Chhetri, P.; Düllmann, C. E.; Ezold, J. G.; Gadelshin, V.; Gaiser, A. N.; Giacoppo, F.; Heinke, R.; et al. Atomic-Structure Investigations of Neutral Einsteinium by Laser Resonance Ionization. *Phys. Rev. Res.* 2022, *4*, No. 043053.

(99) Chhetri, P.; Ackermann, D.; Backe, H.; Block, M.; Cheal, B.; Droese, C.; Düllmann, C. E.; Even, J.; Ferrer, R.; Giacoppo, F.; et al. Precision Measurement of the First Ionization Potential of Nobelium. *Phys. Rev. Lett.* 2018, *120*, 263003.

(100) Sato, T. K.; Asai, M.; Borschevsky, A.; Beerwerth, R.; Kaneya, Y.; Makii, H.; Mitsukai, A.; Nagame, Y.; Osa, A.; Toyoshima, A.; et al. First Ionization Potentials of Fm, Md, No, and Lr: Verification of Filling-Up of 5f Electrons and Confirmation of the Actinide Series. *J. Am. Chem. Soc.* 2018, *140*, 14609−14613.

(101) Myasoedov, F. B.; Kirby, H. W.; Tananaev, I. G. Protactinium. In *The Chemistry of the Actinide and Transactinide Elements*, 4th ed.; Morss, L. R., Edelstein, N. M., Fuger, J., Eds.; Springer, Dordrecht, The Netherlands, 2010; pp 161−252.